Synthesis and characterization of zinc ferrite nanoparticles by a thermal treatment method

ARTICLE *in* SOLID STATE COMMUNICATIONS · JULY 2011

Impact Factor: 1.9 · DOI: 10.1016/j.ssc.2011.04.018

Solid State Communications 151 (2011) 1031–1035

Contents lists available at ScienceDirect

Solid State Communications

journal homepage: www.elsevier.com/locate/ssc

Synthesis and characterization of zinc ferrite nanoparticles by a thermal treatment method

Mahmoud Goodarz Naseri [a,b,*], Elias B. Saion [a], Mansor Hashim [a,c], Abdul Halim Shaari [a], Hossein Abasstabar Ahangar [d]

[a] Department of Physics, Universiti Putra Malaysia, 43400 UPM Serdang, Selangor, Malaysia
[b] Department of Physics, Faculty of Science, Malayer University, Malayer, Iran
[c] Advanced Materials and Nanotechnology Laboratory, Institute of Advanced Technology, Malaysia
[d] Department of Chemistry, Universiti Putra Malaysia, 43400 UPM Serdang, Selangor, Malaysia

ARTICLE INFO

Article history:
Received 18 January 2011
Received in revised form
18 April 2011
Accepted 21 April 2011
by E.V. Sampathkumaran
Available online 5 May 2011

Keywords:
A. Zinc ferrite
D. Magnetic properties
E. Thermal treatment

ABSTRACT

Crystalline zinc ferrite ($ZnFe_2O_4$) was prepared by the thermal treatment method, followed by calcination at various temperatures from 723 to 873 K. Poly (vinyl pyrrolidon) (PVP) was used as a capping agent to stabilize the particles and prevent them from agglomeration. The characterization studies were conducted by X-ray diffraction (XRD) and transmission electron microscopy (TEM). The average particle sizes of 17–31 nm were obtained by TEM images, which were in good agreement with the XRD results. Fourier transform infrared spectroscopy (FT-IR) confirmed the presence of metal oxide bands at all temperatures and the absence of organic bands at 873 K. The magnetic properties were demonstrated by a vibrating sample magnetometer (VSM), which displayed super paramagnetic behaviors for the calcined samples. The present study also substantiated that, in ferrites, the values of the quantities that were acquired by VSM, such as the saturation magnetization and coercivity field, are primarily dependent on the methods of preparation of the ferrites. Electron paramagnetic resonance (EPR) spectroscopy showed the existence of unpaired electrons and measured the peak-to-peak line width (ΔH_{pp}), the resonant magnetic field (H_r), and the g-factor values.

1. Introduction

Currently, magnetic oxide nanoparticles are attracting significant interest due to their extensive applications, ranging from fundamental research to industrial use. Spinel ferrite nanocrystals are regarded as two of the most important inorganic nanomaterials because of their electronic, optical, electrical, magnetic, and catalytic properties. Spinel ferrites have the structure AB_2O_4 in which A and B display tetrahedral and octahedral cation sites, respectively, and O indicates the oxygen anion site. Metal spinel ferrite nanoparticles have the general molecular formula MFe_2O_4 (e.g., M = Zn, Ni, Co, Mn, or Mg), and they have a face-centered-cubic (fcc) close packing structure. Among the spinel ferrite compounds, zinc ferrite ($ZnFe_2O_4$) has been studied extensively due to its high electromagnetic performance, excellent chemical stability, mechanical hardness, low coercivity, and moderate saturation magnetization, which make it a good contender for applications as soft magnets and low-loss materials at high frequencies [1–3].

These properties are dependent on the chemical composition and microstructural characteristics in which the particle size and shape might be controlled in the fabrication processes. In order to achieve materials that have the desired physical and chemical properties, the preparation of zinc ferrite nanocrystals through different routes has become an essential focus of the related research and development activities. Various fabrication methods to prepare spinel zinc ferrite nanocrystals have been reported, e.g., sol–gel methods [4], the ball-milling technique [5], co-precipitation [6], the aerogel process [7], the hydrothermal method [8], the reverse micelles process [9], and the microemulsion method [10]. Various precipitation agents have been used to produce specific size and shape zinc ferrite nanocrystals, e.g., metal hydroxide in the co-precipitation method, surfactant and ammonia in the reverse micelles process and various microemulsion methods, and organic matrices in the sol–gel method. Most of these methods have achieved particles of the required sizes and shapes, but they are difficult to employ on a large scale because of their expensive and complicated procedures, high reaction temperatures, long reaction times, toxic reagents and by-products, and their potential harm to the environment.

In the present study, zinc ferrite nanocrystals were prepared from an aqueous solution containing metal nitrates, poly (vinyl

* Corresponding address: Department of Physics, Universiti Putra Malaysia, 43400 UPM Serdang, Selangor, Malaysia. Tel.: +60 142698153; fax: +60 389454454.
E-mail address: mahmoud.naseri55@gmail.com (M.G. Naseri).

0038-1098/$ – see front matter © 2011 Elsevier Ltd. All rights reserved.
doi:10.1016/j.ssc.2011.04.018

pyrrolidon), and deionized water using a low temperature thermal treatment method, followed by grinding and calcination. No other chemicals were added to the solution. This method is environmentally friendly in that it neither uses nor produces toxic substances, and it offers the advantages of simplicity, low cost, and low reaction temperatures. The textural and morphological characteristics of the zinc ferrite nanocrystals we prepared were studied with various techniques to determine the influence of calcination temperature on the crystallization, morphology, and particle size distribution of the nanocrystals and to explore other parameters of interest.

2. Experimental

Metal nitrate reagents, poly (vinyl pyrrolidon) (PVP), and deionized water were used as precursors. In addition, a capping agent to control the agglomeration of the particles and a solvent were used. Iron nitrate, $Fe(NO_3)3 \bullet 9H_2O$, and zinc nitrate, $Zn(NO_3)2 \bullet 6H_2O$, were purchased from Acros Organics with a purity exceeding 99%. PVP (MW = 29 000) was purchased from Sigma Aldrich and was used without further purification. An aqueous solution of PVP was prepared by dissolving 4 g of polymer in 100 ml of deionized water at 363 K, before mixing 0.2 mmol iron nitrate and 0.1 mmol zinc nitrate (Fe:Zn = 2:1) into the polymer solution and constantly stirring for 2 h using a magnetic stirrer until a colorless, transparent solution was obtained. A glass electrode was used to determine the pH of the solution, which ranged 1–2. No precipitation of materials was observed before the heat treatment. The mixed solution was poured into a glass Petri dish and heated at 353 K in an oven for 24 h to evaporate the water. The dried, orange, solid zinc ferrite that remained was crushed and ground in a mortar to form powder. The calcinations of the powders were conducted at 723, 773, 823 and 873 K for 3 h for the decomposition of organic compounds and the crystallization of the nanocrystals.

3. Characterization

The structure of the $ZnFe_2O_4$ nanoparticles was characterized by the XRD technique using a Shimadzu diffract meter model XRD 6000 employing Cu K_α (0.154 nm) radiation to generate diffraction patterns from powder crystalline samples at ambient temperature in a 2θ range of 10°–70°. The microstructure and particle size of the nanocrystals were determined from Transmission Electron Microscopy (TEM) images that were obtained by using a JEOL 2010F UHR version electron microscope at an accelerating voltage of 200 kV. FT-IR spectra were recorded using a PerkinElmer FT-IR model 1650 spectrometer. Before recording the spectra, the samples were placed on a Universal ATR Sampling Accessory (diamond coated with CsI) and pressed, and then the spectra were recorded. Magnetization measurements were conducted using a vibrating sample magnetometer (VSM) (Lake Shore 4700) at room temperature with a maximum magnetic field of 15 kOe. Electron paramagnetic resonance (EPR) spectra were recorded on a JEOL JES-FA200 EPR spectrometer (JEOL, Tokyo, Japan) at room temperature.

4. Results and discussion

Fig. 1 shows the interactions between the PVP as a capping agent [11] and the metal ion precursors. Fig. 1 shows that the zinc (II) and iron (III) ions are bound by the strong ionic bonds between the metallic ions and the amide group in a polymeric chain or between the polymeric chains. This uniform immobilization of metallic ions in the cavities of the polymer chains favors the formation of a uniformly-distributed, solid solution of the metallic oxides in the calcination process

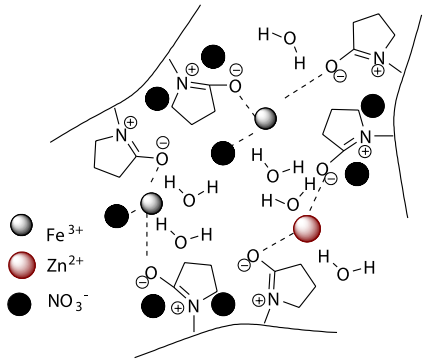

Fig. 1. A proposed mechanism of interactions between PVP and metal ions before calcination.

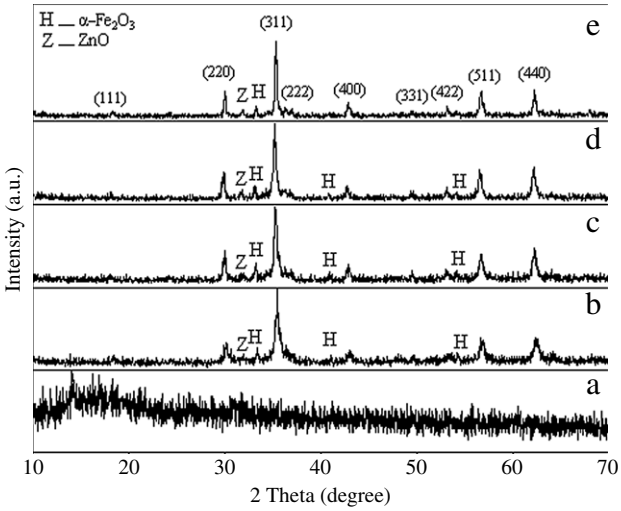

Fig. 2. XRD patterns of precursor and zinc ferrite nanoparticles calcined at (a) 723, (b) 773, (c) 823 and (d) 873 K.

The XRD diffraction patterns of the precursor and zinc ferrite nanoparticles are shown in Fig. 2. A broad peak occurred in the precursor (Fig. 2(a)), which does not have sharp diffraction patterns and is still amorphous. The calcined patterns show the reflection planes (111), (220), (311), (222), (400), (331), (422), (511) and (440), which confirm the presence of single-phase $ZnFe_2O_4$ with a face-centered cubic structure [12]. Except for the impure phases of α-Fe_2O_3 and ZnO, which are found in all calcined samples and occur naturally as hematite and zincite, respectively [13,14], the remaining peaks correspond to the standard pattern of $ZnFe_2O_4$ (cubic, $a = 0.8441$ nm, space group: $Fd3m$, $Z = 8$; ICDD PDF: 22-1012). The results obtained from XRD were analyzed using the Chekcell program, which calculated lattice parameters of 0.8498 ± 0.0041, 0.8468 ± 0.0028, 0.8471 ± 0.0037 and 0.8479 ± 0.0014 nm for the samples calcined at 723, 773, 823 and 873 K, respectively (Table 1). These values are slightly greater than the lattice parameters that have been previously reported for the standard pattern above.

The XRD results were analyzed by the Scherer formula:

$$D = 0.9\lambda/(\beta \cos\theta),$$

where D is the crystallite size (nm), β is the full width of the diffraction line at half the maximum intensity measured in radians, λ is the X-ray wavelength, and θ is the Bragg angle [15]. This formula was used to estimate the average particle sizes, which ranged from 21 nm at 723 K to 33 nm at 873 K, as listed in Table 1.

Fig. 3(a) shows the FT-IR spectrum of the precursor in the wave-number range between 280 and 4000 cm^{-1}. The bands

Table 1
Average particle sizes (nm) of zinc ferrite nanoparticles determined from XRD and TEM and magnetic properties observed from VS and ESR techniques at room temperature.

Specimens $ZnFe_2O_4$	Calcination temperature (K)	Average particle size XRD (nm)	Average particle size TEM (nm)	Lattice parameter (nm)	Saturation magnetization M_s (emu/g)	Magnetic resonance field H_r (Oe)	Gromagnetic ratio (g-values)	Linewidth ΔH_{pp} (Oe)
Zn Ferrite 1	723	21	17 ± 7	0.8498	4.49	–	–	–
Zn Ferrite 2	773	24	22 ± 2.5	0.8468	2.66	3137	2.0311	498
Zn Ferrite 3	823	31	27 ± 5	0.8471	1.81	3131.5	2.0667	621
Zn Ferrite 4	873	33	31 ± 11	0.8479	0.74	3122	2.1204	728

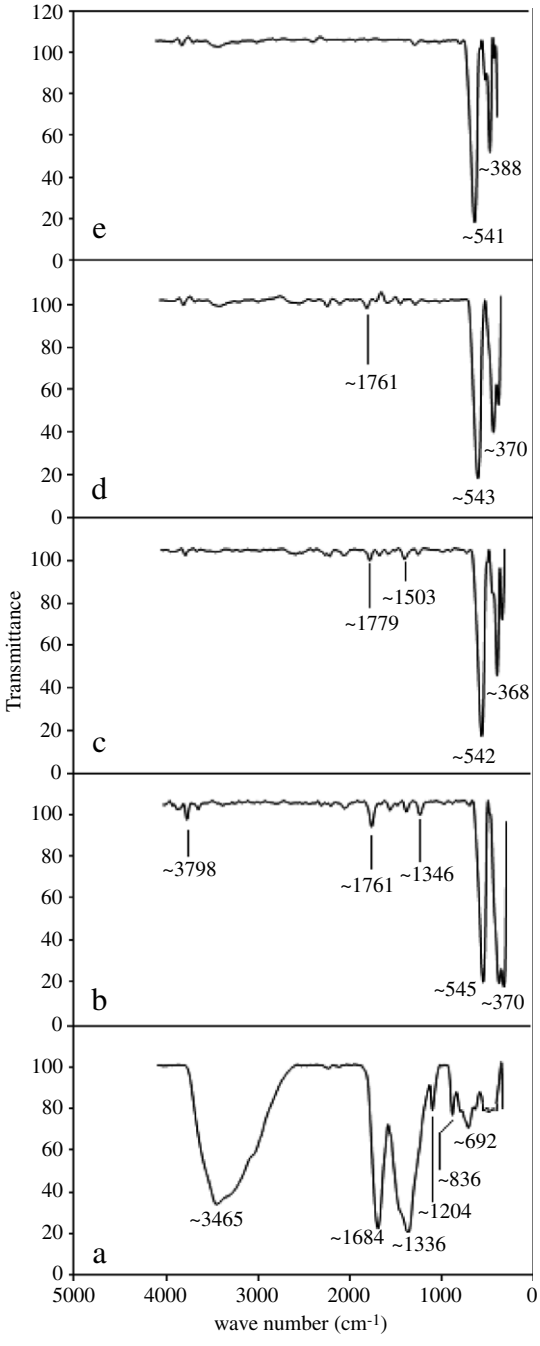

Fig. 3. FT-IR spectra of precursor and zinc ferrite nanoparticles calcined at (a) 723, (b) 773, (c) 823 and (d) 873 K.

with peaks at 692 and 836 cm^{-1} were assigned to the formation vibration of C–N=O bending and the C–C ring, respectively. The band at 1204 cm^{-1} was associated with C–N stretching vibration, and the appearance of the band at 1336 cm^{-1} was attributed to C–H bending vibration from the methylene groups. Finally, there were bands at 1684 cm^{-1} and 3465 cm^{-1}, which were associated with C=O stretching vibration and N–H stretching vibration, respectively [16].

The vibrational spectra of the absorption bands of pure spinel zinc ferrite nanoparticles were observed at 388 and 541 cm^{-1} for the samples calcined at 873 K (Fig. 3(e)). This indicated the formation of the spinel $ZnFe_2O_4$ nanostructure as suggested by previously published data [13]. The IR bands of solids are usually assigned to the vibration of ions in the crystal lattice. For the samples calcined at 873 K, the absence of peaks in the ranges of 1000–1300 cm^{-1} and 2000–3000 cm^{-1} confirmed the non-existence of the O–H mode, C–O mode, and C=H stretching mode of organic sources [16]. This IR analysis was very useful for establishing the calcination temperature of 873 K because it removed unwanted ions that may pollute the crystal lattice during preparation. However, at calcination temperatures of less than 873 K (Fig. 2(d)), there was still a trace of a broadband absorption peak at 1761 cm^{-1} due to ester formation as a consequence of the scission of the N–C=O bond [17]. The FT-IR spectra (Fig. 3(b) and (c)) show the existence of absorption bands at 370 and 368 cm^{-1} and at 545 and 542 cm^{-1}, which are attributed to Zn ↔ O and Fe ↔ O bonds, respectively, and they also show that there are organic compounds in the samples, as confirmed by the appearance of the peaks at 1346, 1761, and 3798 cm^{-1} (Fig. 3(b)) and at 1503 and 1779 cm^{-1} (Fig. 3(c)).

The TEM images in Fig. 4 show the size, shape, and distribution of zinc ferrite samples at different calcination temperatures from 723 to 873 K. The results indicate that the samples prepared by the thermal treatment method were uniform in morphology and particle size distribution. The particle size increased with increasing calcination temperature (Table 1). The smallest particle size obtained in this study was 17 nm at 723 K, and the largest was 31 nm at the highest calcination temperature (873 K). This suggested that several neighboring particles fused together to increase the particle size by the melting of their surfaces [18]. Particle size enlargement due to grain growth has been observed previously in cobalt ferrite [19] and in nickel ferrite [20] systems at higher calcination temperatures.

Fig. 5 shows the magnetization curves of zinc ferrite nanoparticles at (a) 723, (b) 773, (c) 823 and (d) 873 K, which were measured at room temperature in the range of approximately −15 to +15 kOe. Their coercivity fields (H_c) are almost negligible, and all of them exhibit super-paramagnetic behaviors. Table 1 provides the values of saturation magnetization (M_s) of the calcined samples, along with calcination temperatures and particle sizes. These data make it clear that different parameters were responsible for the saturation magnetization decreasing from 4.49 to 0.74 emu/g when the particle size increased from 17 to 31 nm. Cation inversion is one of the most important parameters that can be effective in the variation of the magnetic properties of zinc ferrite nanoparticles from the properties of the bulk form of the same material. In bulk form, zinc ferrite has a normal spinel structure in which all Zn^{2+} ions are in A sites and Fe^{3+} ions are distributed in B sites [21]. However, in bulk, zinc ferrite only occurs in intra-sub-lattice (B–B) exchange interactions, and it does not have intra-sub-lattice (A–A)

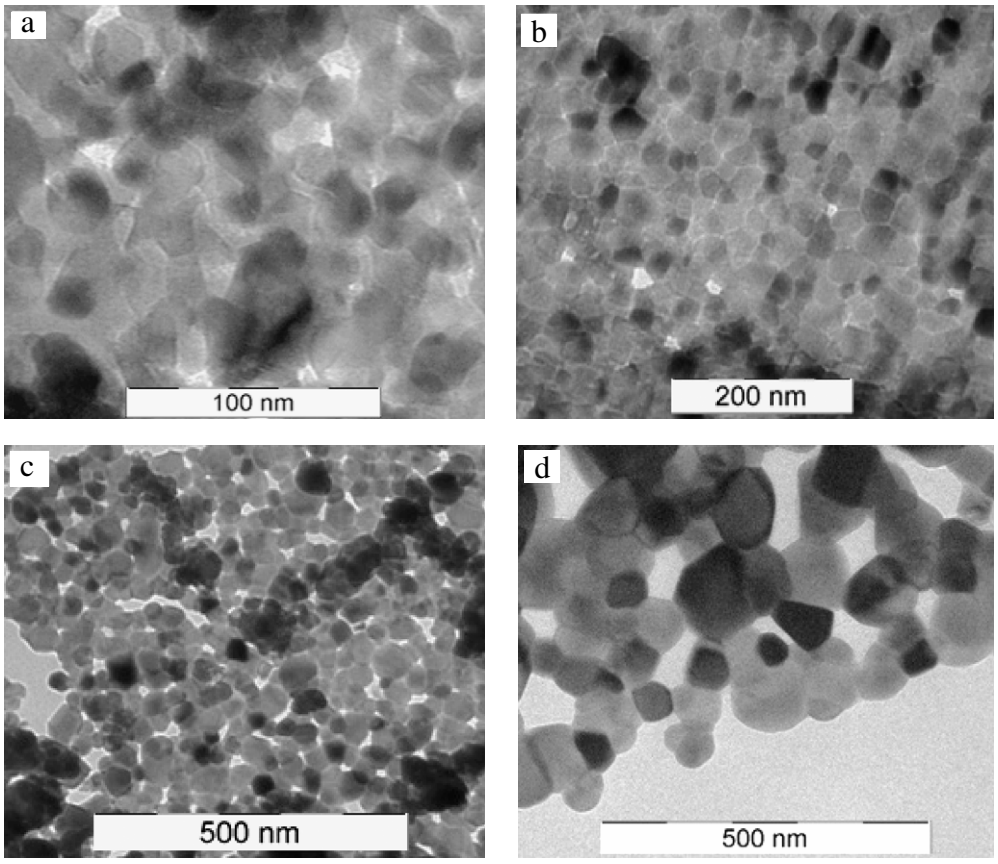

Fig. 4. TEM images of zinc ferrite nanoparticles calcined at (a) 723, (b) 773, (c) 823 and (d) 873 K.

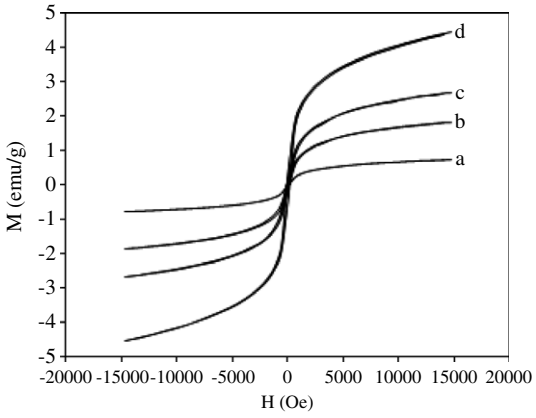

Fig. 5. Magnetization curves at room temperature for zinc ferrite nanoparticles calcined at (a) 723, (b) 773, (c) 823 and (d) 873 K.

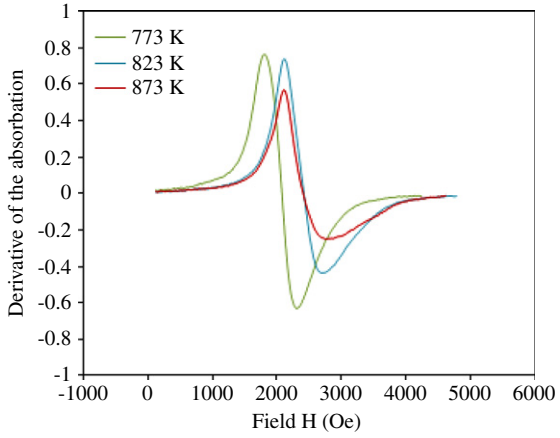

Fig. 6. EPR spectra of zinc ferrite nanoparticles calcined from 773 to 873 K.

exchange interactions or inter-sub-lattice (A–B) super-exchange interactions [22].

Inter-sub-lattice (A–B) super-exchange interactions of the cations are much stronger than the (A–A) and (B–B) interactions [4].

Due to the cation inversion, which originates from thermal and mechanical treatment [23], the structure of $ZnFe_2O_4$ transfers from a normal spinel structure to a mixed spinel structure [22]. This cation inversion causes the zinc ferrite nanoparticles to experience inter-sub-lattice (A–B) super-exchange interactions and intra-sub-lattice (A–A) exchange interactions in addition to intra-sub-lattice (B–B) exchange interactions. But, due to the degree of inversion, which is large for smaller size particles, inter-sub-lattice (A–B) super-exchange interactions in smaller size particles occur to a greater extent than in larger size particles. Hence, the saturation magnetization increases for smaller size particles. Roy et al. [24], using Mossbauer's experiment, showed that the degree of inversion is large in the case of smaller size particles.

Also, an impure α-Fe_2O_3 phase was detected by XRD (Fig. 2), and the surface spin structure can be an influence that increases the saturation magnetization in smaller size particles [13].

It is worth noting that the magnetic properties of similar ferrite nanoparticles of the same particle size differ depending on the preparation method used. Table 2 shows some literature values of M_s and H_c that were measured at similar conditions for some spinel ferrite nanoparticles. The data show that the pairs of similar spinel ferrite nanoparticles of the same particle size have different saturation magnetization values and coercivity fields. The results

Table 2
Some literature values of M_s and H_c for some spinel ferrite nanoparticles that were measured at room temperature in range of approximately −10 to +10 kOe.

Specimens	Preparation method	Average particle size (nm)	Saturation magnetization M_s (emu/g)	Coercivity field H_c (Oe)	References
ZnFerrite	Combustion	20	4	Negligible	[25]
ZnFerrite	Modified sol gel	∼20	1.4	156	[13]
NiFerrite	Sol gel	∼9	32.1	59	[26]
NiFerrite	Coprecipitation	9	11.9	Negligible	[27]
CoFerrite	Mechanic alloying	30	77	2000–2700	[28]
CoFerrite	Hydrothermal	30	30	Negligible	[29]

indicate that, in fact, the magnetic properties of ferrites are related primarily to the methods used to prepare them.

Fig. 6 shows the EPR spectra of the samples calcined at (a) 773, (b) 823 and (c) 873 K exhibited broad, symmetrical signals.

Peak-to-peak line width (ΔH_{pp}), resonant magnetic field (H_r), and g-factor are three parameters that characterize the magnetic properties. It is obvious from Table 1 that the values of ΔH_{pp} increase from 498 to 728 Oe and the values of g-factor increase from 2.03 to 2.12 when the calcination temperature and particle size were increased. In ferrites, variations of ΔH_{pp} and g-factor can be due to dipole–dipole interactions and super-exchange interactions [30].

Table 1 also shows that the value of the resonant magnetic field decreased from 3137 to 3122 Oe as the calcination temperature increased. According to the equation:

$$g = h\nu/\beta H$$

where h is Planck's constant, ν is the microwave frequency, β is the Bohr magneton (9.274×10^{-21} erg Oe^{-1}), and H is resonant magnetic field, the resonance magnetic field should decrease when the g-factor increases, whereas ν is constant in EPR spectroscopy. The addition of Fe^{3+} ions to an A site, as was discussed in the last part, causes an increase in the super-exchange interactions, contributing to the increase of the internal field and the decrease of the resonance magnetic field [25]. Increases in ΔH_{pp} and g-factor and decreases in H_r with increasing calcination magnetization values have been reported in mixed $NiFe_2O_4$ nanoparticles [31].

5. Conclusions

The results of this investigation indicate that the thermal treatment method can be used for synthesizing $ZnFe_2O_4$ nanoparticles using poly (vinyl pyrrolidon) as a capping agent to stabilize the particles and prevent them from agglomerating. XRD patterns and TEM images show the formation of $ZnFe_2O_4$ nanoparticles. An increase in particle size from 17 to 31 nm was observed by increasing the calcination temperature from 723 to 873 K. The FT-IR spectrum confirmed the presence of metal oxides at all temperatures, but organic compounds (PVP) were removed completely at 873 K. Magnetic results were obtained by VSM, and they showed that saturation magnetization decreased when the particle sizes increased, whereas the coercivity field was negligible, and all of the samples displayed super-paramagnetic behaviors. The study also substantiated that, in ferrites, the values of the quantities that were acquired by VSM, such as saturation magnetization and coercivity field, are primarily dependent on the methods of preparation of these ferrites. Electron paramagnetic resonance (EPR) spectroscopy showed the existence of unpaired electrons and measured peak-to-peak line width (ΔH_{pp}), resonant magnetic field (H_r), and the g-factor values. This simple method, which is cost-effective and environmentally friendly, produces no toxic byproducts and can be used to fabricate pure, crystalline spinel zinc ferrite nanocrystals. Furthermore, this method can be extended to the synthesis of other spinel ferrite nanoparticles of interest.

Acknowledgments

The authors would like to thank Miss Fatemeh Moazami Goodarzi for her great assistance in the chemical mechanism study. This work was supported by the Ministry of Higher Education of Malaysia under the FRGS grant and Universiti Putra Malaysia under the RUGS grant.

References

[1] G. Maggioni, A. Vomiero, S. Carturan, C. Scian, G. Mattei, M. Bazzan, C.J. Fernandez, P. Mazzoldi, A. Quaranta, G.D. Mea, Appl. Phys. Lett. 85 (2004) 5712–5714.
[2] K.A. Bogle, S.D. Dhole, V.N. Bhoraskar, Nanotechnology 17 (2006) 3204–3208.
[3] P. Gangopadhyay, R. Kesavmoorthy, S. Bera, P. Magudapathy, K.G.M. Nair, B.K. Panigrahi, S. Narasimhan, Phys. Rev. Lett. 94 (2005) 47403–47404.
[4] M. Atif, S.K. Hasanain, M. Nadeem, J. Sci. Commun. 138 (2006) 416–421.
[5] J.Z. Jiang, P. Wynn, S. Morup, T. Okada, F.J. Berry, Nanostruct. Mater. 12 (1999) 737–740.
[6] S.D. Shenoy, P.A. Joy, M.R. Anantharaman, J. Magn. Magn. Mater. 269 (2004) 217–226.
[7] H.H. Hamdeh, J.C. Ho, S.A. Oliver, R.J. Willey, G. Oliveri, G. Busca, J. Appl. Phys. 81 (4) (1997) 1851–1858.
[8] S.H. Yu, T. Fujino, M. Yoshimura, J. Magn. Magn. Mater. 256 (2003) 420–424.
[9] S.A. Morrison, C.L. Cahill, E.E. Carpenter, S. Calvin, R. Swaminathan, M.E. McHenry, V.G. Harris, J. Appl. Phys. 95 (2004) 6392–6395.
[10] J.F. Hochepied, P. Bonville, M.P. Pileni, J. Phys. Chem. B 104 (2000) 905–912.
[11] P. Sivakumar, R. Ramesh, A. Ramanand, S. Ponnusamy, C. Muthamizhchelvan, Mater. Lett. 65 (2011) 483–485.
[12] C.N. Chinnasamy, A. Narayanasamy, N. Ponpandian, K. Chattopadhyay, H. Gu'erault, J.M. Greneche, J. Phys.: Condens. Matter 12 (2000) 7795–7805.
[13] P. Laokul, V. Amornkitbamrung, S. Seraphin, S. Maensiri, Curr. Appl. Phys. 11 (2011) 101–108.
[14] J.P. Singh, R.S. Payal, R.C. Srivastava, H.M. Agrawal, P. Chand, A. Tripathi, R.P. Tripathi, J. Phys. Conf. Ser. 217 (2010) 012108.
[15] B.D. Cullity, Elements of X-ray Diffraction, 2nd ed., Addison-Wesley, London, 1978, p. 102.
[16] M.I. Loría-Bastarrachea, W. Herrera-Kao, J.V. Cauich-Rodríguez, J.M. Cervantes-Uc, H. Va'zquez-Torres, A.A. vila-Ortega, J. Therm. Anal. Calorim. (2010) doi:10.1007/s10973-010-1061-9.
[17] G. Bianco, M.S. Soldi, E.A. Pinheiro, A.T.N. Pires, M.H. Gehlen, V. Soldi, 80 (2003) 567–574.
[18] Y. Qu, H. Yang, N. Yang, Y. Fan, H. Zhu, G. Zou, Mater. Lett. 60 (2006) 3548–3552.
[19] K. Maaz, A. Mumtaz, S.K. Hasanain, A. Ceylan, J. Magn. Magn. Mater. 308 (2007) 289–295.
[20] T. Giannakopoulou, L. Kompotiatis, A. Kontogeorgakos, G. Kordas, J. Magn. Magn. Mater. 246 (2002) 360–365.
[21] D.S. Mathew, R.S. Juang, Chem. Eng. J. 129 (2007) 51–65.
[22] F.S. Li, L. Wang, J.B. Wang, Q.G. Zhou, X.Z. Zhou, H.P. Kunkel, G. Williams, J. Magn. Magn. Mater. 268 (2004) 332–339.
[23] J.P. Singh, R.C. Srivastava, H.M. Agrawal, R. Kumar, Nucl. Instrum. Methods Phys. Res. B 268 (2010) 1422–1426.
[24] M.K. Roy, B. Haldar, H.C. Verma, Nanotechnology 17 (2006) 232–237.
[25] P. Priyadharsini, A. Pradeep, P.S. Rao, G. Chandrasekaran, Mater. Chem. Phys. 116 (2009) 207–213.
[26] M. George, A.M. John, S.S. Nair, P.A. Joy, M.R. Anantharaman, J. Magn. Magn. Mater. 302 (2006) 190–195.
[27] V. Sepelak, M. Menzel, I. Bergmann, M. Wiebcke, F. Krumeich, K.D. Becker, J. Magn. Magn. Mater. 272–276 (2004) 1616–1618.
[28] D. Zhao, X. Wu, H. Guan, E. Han, J. Supercrit. Fluids 42 (2007) 226–233.
[29] H. Chaoquan, G. Zhenghong, Y. Xiaorui, J. Magn. Magn. Mater. 320 (2008) L70–L73.
[30] G. Vaidyanathana, S. Sendhilnathan, Physica B 403 (2008) 2157–2167.
[31] S.S. Umare, R.S. Ningthoujam, S.J. Sharma, S. Shrivastava, S. Kurian, N.S. Gajbhiye, Hyperfine Interact. 184 (2008) 235–243.